Impaired Malate and Fumarate Accumulation Due to the Mutation of the Tonoplast Dicarboxylate Transporter Has Little Effects on Stomatal Behavior[1]

David B. Medeiros,[a,b,c] Kallyne A. Barros,[a,b] Jessica Aline S. Barros,[a,b] Rebeca P. Omena-Garcia,[a,b] Stéphanie Arrivault,[c] Lílian M. V.P. Sanglard,[b] Kelly C. Detmann,[b] Willian Batista Silva,[a,b] Danilo M. Daloso,[c,2] Fábio M. DaMatta,[b] Adriano Nunes-Nesi,[a,b] Alisdair R. Fernie,[c] and Wagner L. Araújo[a,b,3]

[a]Max-Planck Partner Group at the Departamento de Biologia Vegetal, Universidade Federal de Viçosa, 36570-900 Viçosa, Minas Gerais, Brazil
[b]Departamento de Biologia Vegetal, Universidade Federal de Viçosa, 36570-900 Viçosa, Minas Gerais, Brazil
[c]Max Planck Institute of Molecular Plant Physiology, 14476 Potsdam-Golm, Germany

ORCID IDs: 0000-0001-9086-730X (D.B.M.); 0000-0003-1842-420X (D.M.D.); 0000-0002-4796-2616 (W.L.A.).

Malate is a central metabolite involved in a multiplicity of plant metabolic pathways, being associated with mitochondrial metabolism and playing significant roles in stomatal movements. Vacuolar malate transport has been characterized at the molecular level and is performed by at least one carrier protein and two channels in Arabidopsis (*Arabidopsis thaliana*) vacuoles. The absence of the Arabidopsis tonoplast Dicarboxylate Transporter (tDT) in the *tdt* knockout mutant was associated previously with an impaired accumulation of malate and fumarate in leaves. Here, we investigated the consequences of this lower accumulation on stomatal behavior and photosynthetic capacity as well as its putative metabolic impacts. Neither the stomatal conductance nor the kinetic responses to dark, light, or high CO_2 were highly affected in *tdt* plants. In addition, we did not observe any impact on stomatal aperture following incubation with abscisic acid, malate, or citrate. Furthermore, an effect on photosynthetic capacity was not observed in the mutant lines. However, leaf mitochondrial metabolism was affected in the *tdt* plants. Levels of the intermediates of the tricarboxylic acid cycle were altered, and increases in both light and dark respiration were observed. We conclude that manipulation of the tonoplastic organic acid transporter impacted mitochondrial metabolism, while the overall stomatal and photosynthetic capacity were unaffected.

Malate is a central metabolite in all plant species, fulfilling a multiplicity of functions as both an intermediate of the tricarboxylic acid cycle (Fernie et al., 2004) and carbon skeletons exported from the mitochondrion supporting amino acid biosynthesis (Tronconi et al., 2008). Malate also is involved in several processes including cellular pH regulation (Hurth et al., 2005), partial control over nutrient uptake (Weisskopf et al., 2006), aluminum tolerance (Delhaize et al., 2007), pathogen response (Bolwell et al., 2002), and stomatal movements (Hedrich et al., 1994). Moreover, it has been demonstrated to be a transcriptional regulator in metabolite signaling (Finkemeier et al., 2013), an important carbon storage molecule in C3 plants (Zell et al., 2010), and a key component of photosynthesis in C4 and Crassulacean acid metabolism plants (Maier et al., 2011).

Vacuolar malate transport, which has been characterized at the molecular level, is thought to be essential to maintain normal cellular function (Emmerlich et al., 2003). First, the gene encoding the vacuolar malate transporter, a plant homolog to the human sodium ion/dicarboxylate cotransporter, the tDT (tonoplast Dicarboxylate Transporter), was identified in Arabidopsis (*Arabidopsis thaliana*). The *tdt* knockout mutants are deficient in vacuolar malate transport activity, exhibited substantially reduced levels of malate and fumarate in the leaves, and isolated vacuoles from these mutants were highly impaired in the import of [^{14}C]malate yet

[1] This work was supported by funding from the Max Planck Society, the CNPq (National Council for Scientific and Technological Development, Brazil, Grant 402511/2016-6), and the FAPEMIG (Foundation for Research Assistance of the Minas Gerais State, Brazil, Grants APQ-01078-15 and APQ-01357-14) to W.L.A. Scholarships granted by FAPEMIG to D.B.M. (BDS-00020-16), by CNPq to K.A.B. and J.A.S.B., as well as research fellowships granted by CNPq-Brazil to A.N.N. and W.L.A. are also gratefully acknowledged.

[2] Current address: Departamento de Bioquímica e Biologia Molecular, Universidade Federal do Ceará, Fortaleza, 60440-970 Ceará, Brazil.

[3] Address correspondence to wlaraujo@ufv.br.

The author responsible for distribution of materials integral to the findings presented in this article in accordance with the policy described in the Instructions for Authors (www.plantphysiol.org) is: Wagner L. Araújo (wlaraujo@ufv.br).

D.B.M., A.R.F., and W.L.A. designed the research; D.B.M. performed most of the research with the support of K.A.B., J.A.S.B., R.P.O.G., S.A., L.M.V.P.S., and K.C.D.; W.B.S., D.M.D., A.N.N., and F.M.D. contributed new reagents/analytic tools; A.N.N., F.M.D., and S.A. analyzed the data, discussed the results, and complemented the writing; D.B.M., A.R.F., and W.L.A. analyzed the data and wrote the article, which was later approved by all the others.

www.plantphysiol.org/cgi/doi/10.1104/pp.17.00971

respired exogenously applied [^{14}C]malate faster than wild-type plants (Emmerlich et al., 2003). However, in contrast to its homolog in animal cells, the plant protein resides at the tonoplast, and the transport of malate by the tDT is not sodium dependent (Emmerlich et al., 2003). In addition, Hurth et al. (2005) demonstrated that tDT is critical for the regulation of pH homeostasis under altered pH conditions. These authors further suggested that Arabidopsis vacuoles contain at least two types of carrier proteins and a channel for the transport of dicarboxylates and citrate, thus providing the metabolic flexibility needed by plants to respond to different environmental circumstances. A member of the aluminum-malate transporter (ALMT) family, ALMT9, was the first channel characterized to mediate malate and fumarate currents directed into the vacuole of mesophyll cells in Arabidopsis (Kovermann et al., 2007). However, it was later demonstrated to mediate malate-induced chloride currents that also are important for stomatal opening (De Angeli et al., 2013). A second member of the ALMT family, ALMT6, mediates Ca^{2+}- and pH-dependent malate currents into guard cell vacuoles (Meyer et al., 2011). Despite *ALMT6* expression being much higher in guard cells than in the mesophyll, suggesting an important role of this channel in stomatal movements, no obvious stomatal or growth phenotype was observed under optimal growth conditions (Meyer et al., 2011).

The accumulation of malate either in guard cell cytosol and vacuoles or in the apoplastic space can impact stomatal movements and also regulate the activity of anion channels at guard cell plasma or vacuolar membrane (Hedrich and Marten, 1993; Hedrich et al., 1994; Raschke, 2003; Lee et al., 2008; Negi et al., 2008; Kim et al., 2010; De Angeli et al., 2013). Indeed, the role of organic acids (e.g. malate and fumarate) in the regulation of guard cell movements occurs not only by providing the osmotic control but also by playing a critical role in meeting the energetic demand of the guard cells (Santelia and Lawson, 2016). This fact apart, our knowledge about the metabolic hierarchy regulating guard cells movements in response to changes in organic acids remains fragmentary. Interestingly, further evidence supporting the involvement of organic acid metabolism in leaves by linking mitochondrial metabolism and stomatal function has been demonstrated (Nunes-Nesi et al., 2007; Araújo et al., 2011). Tomato (*Solanum lycopersicum*) plants with constitutively reduced expression of *SlSDH2-2*, which encodes the iron-sulfur subunit of succinate dehydrogenase, presented increased stomatal conductance and photosynthesis mediated by organic acid effects on the stomata (Araújo et al., 2011). Importantly, no effects were observed when the antisense construct for *SlSDH2-2* was expressed under the control of the guard cell-specific *MYB60* promoter (Araújo et al., 2011). By contrast, the constitutive inhibition of the mitochondrial fumarase in tomato plants decreased photosynthesis as a result of impaired stomatal function (Nunes-Nesi et al., 2007).

In an attempt to investigate whether the lower levels of malate and fumarate observed in the *tdt* knockout plants have a greater impact on stomatal movement or mitochondrial metabolism in Arabidopsis, we here combined a range of physiological and biochemical approaches. Our results provide evidence that the manipulation of organic acid tonoplastic transport by suppressing tDT greatly impacts mitochondrial metabolism but has only minor effects on stomatal and photosynthetic capacity. When considered in the context of current knowledge concerning the compartmentation of these metabolites (Gerhardt et al., 1987; Winter et al., 1993, 1994; Hedrich et al., 1994; Martinoia and Rentsch, 1994; Lohaus et al., 2001), this observation suggests that, following the mobilization of the vacuolar malate pool to the cytosol, it is preferentially exported to the apoplast and used to support mitochondrial respiration.

RESULTS

tdt Plants Exhibit a Small Reduction in Vegetative Growth under Short-Day Conditions

Plants lacking a functional tDT display lower levels of malate and fumarate in leaves and isolated vacuoles (Emmerlich et al., 2003; Hurth et al., 2005). Given that these organic acids serve as important carbon storage molecules also in Arabidopsis plants (Zell et al., 2010), we investigated whether the loss of function of *tDT* affects growth in two independent *tdt* T-DNA insertion lines (*tdt-1* and *tdt-2*). We initially confirmed the absence of *tDT* transcripts in leaves of the mutants by reverse transcription PCR (Supplemental Fig. S1). Interestingly, no changes in growth were observed under neutral day conditions (12 h/12 h), with no differences in the rosette fresh weight between wild-type and *tdt* mutant plants (Supplemental Fig. S2A). However, under short-day conditions (8 h/16 h), the mutant lines displayed a slightly reduction in their growth, being characterized by lower rosette fresh weight (Supplemental Fig. S2B). To investigate this apparent growth phenotype further, we evaluated in detail the growth pattern and the metabolism of the genotypes only under short-day conditions. We observed that *tdt* plants presented reductions in the rosette and leaf dry mass, total LA, and rosette area but no significant differences in SLA (Table I). We additionally evaluated the stomatal density and stomatal index, with both being unaltered in the mutant lines under short-day conditions (Table I).

Lack of tDT Has Little Effect on Stomatal Responses to Different Stimuli

Altered organic acid accumulation impacts stomatal behavior coupling mesophyll mitochondrial activity to stomata and, subsequently, to plant growth (Nunes-Nesi et al., 2007; Araújo et al., 2011; Medeiros et al.,

Table I. *Growth and morphology parameters in wild-type and tdt mutant plants*

Data presented are means ± SE (n = 6) obtained in two independent assays; values in boldface for *tdt* plants were determined by Student's t test to be significantly different ($P < 0.05$) from the wild type. LA, Total leaf area; LDM, leaf dry mass; RA, rosette area; RDM, rosette dry mass; SD, stomata density; SI, stomatal index; SLA, specific leaf area.

Parameters	Wild Type	*tdt-1*	*tdt-2*
LA (cm^2)	53.8 ± 2.9	**44.1 ± 2.2**	**42.4 ± 2.3**
LDM (mg)	95.9 ± 4.2	**77.1 ± 5.7**	**72.2 ± 4.2**
RA (cm^2)	43.4 ± 1.5	**38.9 ± 1.3**	**34.9 ± 1.7**
RDM (mg)	122.2 ± 4.1	**93.6 ± 6.4**	**88.1 ± 5.5**
SLA ($m^2\ kg^{-1}$)	60.1 ± 1.3	57.9 ± 1.8	56.3 ± 0.9
SD (stomata mm^{-2})	270.9 ± 10.8	288.8 ± 3.4	273.8 ± 1.4
SI (%)	32.9 ± 1.3	31.4 ± 0.5	29.4 ± 0.9

2016). To further assess the impact caused by an altered accumulation of malate and fumarate due to the lack of a functional tDT on stomatal conductance (g_s) in Arabidopsis, we adopted the following complementary approaches. First, we evaluated the stomatal kinetics during dark-to-light and light-to-dark transitions as well as following changes from normal-to-high and high-to-normal CO_2 concentrations. Second, we evaluated the response of intact leaves following incubation with abscisic acid (ABA), malate, fumarate, and citrate individually by isolating epidermal fragments and analyzing stomatal aperture. Surprisingly, the impaired accumulation of malate and fumarate in *tdt* leaves did not compromise the stomatal response to dark, light, or high CO_2 levels (Fig. 1, A–C). Although no statistical differences were observed ($P < 0.05$) in response to light, dark, and CO_2 concentration, we estimated the half-times of the stomatal kinetic curves by fitting the time course of g_s to an exponential model (Martins et al., 2016). Accordingly, the half-times (expressed in min ± SE) for stomatal kinetics curves also were not altered significantly. However, it is noteworthy that the half-time for light-induced stomatal opening in *tdt-2* plants was lower (8.5 ± 0.7), whereas the values for wild-type and *tdt-1* plants were 13.2 ± 2.3 and 12.5 ± 1.5, respectively. For dark-induced stomatal closure, the half-times were only slightly reduced in *tdt-1* (4.5 ± 0.6) and *tdt-2* (4.5 ± 0.5) when compared with the wild type (5.2 ± 1). The half-times following high CO_2-induced stomatal closure also were only slightly changed in *tdt-1* (5 ± 0.9) and *tdt-2* (4.2 ± 0.5) lines compared with wild-type plants (3.2 ± 0.5). During the recovery back to an ambient CO_2 concentration (C_a) of 400 μmol mol^{-1}, while *tdt-1* plants appeared to be slightly faster in stomatal opening (8.5 ± 1.6), *tdt-2* and the wild type presented half-time values of 12.8 ± 2.3 and 13.6 ± 3.9, respectively. Additionally, no effect on the stomatal aperture following the incubation with ABA, malate, or citrate was observed (Fig. 1D).

Given that malate can affect *tDT* transcript accumulation (Emmerlich et al., 2003), first, we decided to evaluate whether *tDT* is expressed in guard cells by comparing its expression level in both guard cell-enriched epidermal fragments and isolated mesophyll cell protoplast; second, we measured the transcript levels of currently known genes related to organic and inorganic ion transport as well as genes involved in guard cell movements. For this purpose, we investigated by quantitative real-time (qRT)-PCR the transcript levels of ion channels and transporters in guard cell-enriched epidermal fragments, including *ALMT6*, *ALMT9*, *QUAC1*, *ABCB14*, *SLAC1*, *AHA1*, *AHA2*, *AHA5*, *KAT1*, *KAT2*, *AKT1*, *TPC1*, and *GORK* (for a complete description, see "Materials and Methods" and Supplemental Table S1). Regarding the *tDT* expression pattern, our results confirmed previous transcriptome data (Bates et al., 2012), which showed higher expression levels in mesophyll cells than in guard cells (Supplemental Figs. S3 and S4A). Furthermore, the transcript levels of the vast majority of the evaluated genes were only marginally altered in *tdt* plants (Supplemental Fig. S5).

To provide further information that could explain the lack of a stomatal phenotype in *tdt* plants, we next quantified the content of organic acids in the apoplastic fluid. To this end, we collected apoplastic fluid at the middle of the light period from completely water-infiltrated leaves by centrifugation and quantified the absolute levels of fumarate, malate, and citrate in the apoplastic fraction by gas chromatography coupled to mass spectrometry (GC-MS). The unchanged fumarate, malate, and citrate levels in the apoplastic fluid (Fig. 2) probably best explain the lack of effect on stomatal function, since the apoplastic solute concentration is of pivotal significance in driving stomatal movements.

Photosynthetic Capacity Is Not Altered in *tdt* Mutant Plants

We decided to perform a full characterization of the photosynthetic capacity of *tdt* plants. In close agreement with the stomatal kinetics, no differences were observed in instantaneous gas-exchange parameters under either growth irradiance (Table II) or saturation irradiance (Supplemental Table S2). By further analyzing A_N under photosynthetically active photon flux density (PPFD) that ranged from 0 to 1,200 μmol $m^{-2}\ s^{-1}$, we observed that mutant plants exhibited unaltered A_N irrespective of the irradiance (Supplemental Table S3). The light-saturated A_N, light saturation, and compensation points, as well as light use efficiency, remained similar among the genotypes (Supplemental Table S3). Additionally, the response of A_N to the internal CO_2 concentration (A_N/C_i curves; Supplemental Fig. S6A) was obtained and then further converted into responses of A_N to chloroplastic CO_2 concentration (A_N/C_c curves; Supplemental Fig. S6B). Under ambient CO_2 concentration (400 μmol mol^{-1}), C_i and C_c estimations in *tdt* lines were similar to those of the wild type (Supplemental Table S4). g_m, estimated by a combination of gas-exchange and chlorophyll *a* fluorescence parameters using two independent methods,

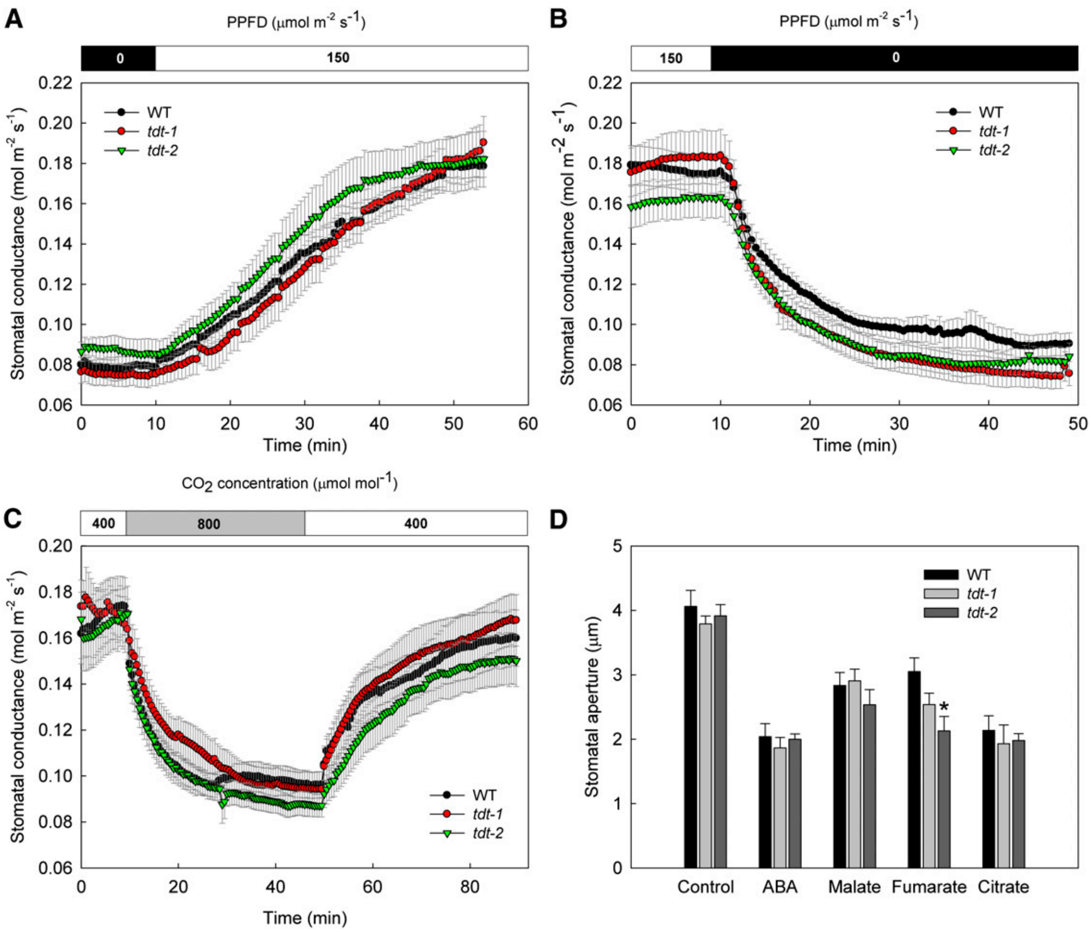

Figure 1. Stomatal responses of *tdt* plants following different stimuli. A to C, Stomatal opening and closing kinetics in response to light and CO_2 concentrations. g_s was evaluated in *tdt-1* and *tdt-2* and the wild type (WT) in response to light (A), dark (B), and CO_2 levels (C). Data presented are means ± SE ($n = 10$). D, Stomatal aperture after incubation with ABA, malate, fumarate, and citrate. The totally expanded fifth leaf of 4-week-old plants was floated on stomatal opening buffer containing 10 mM KCl, 50 μM $CaCl_2$, and 5 mM MES-Tris (pH 6.15) for 2 h in the light (150 μmol m^{-2} s^{-1}) to preopen stomata. Afterward, ABA, malate, fumarate, citrate, or ethanol (solvent control) was added to the opening buffer. After more than 2 h of incubation, the stomatal aperture was examined in the isolated epidermal fragments. Six leaves from different plants were evaluated, and the apertures of at least 20 stomata per leaf were measured, totaling at least 120 stomata per genotype. Data are means ± SE ($n = 6$) obtained in two independent experiments with comparable results. The asterisk indicates a value that was determined by Student's *t* test to be significantly different ($P < 0.05$) from the wild type.

remained unaltered in *tdt* plants (Supplemental Table S4). Accordingly, the maximum carboxylation velocity (V_{cmax}) and maximum capacity for electron transport rate (J_{max}) also were similar between the wild type and mutant lines as a function of both C_i and C_c (Supplemental Table S4).

Mutations in *tDT* Affect Starch, Organic Acid, and Amino Acid Profiles in Both Leaves and Guard Cells

Given that tDT was shown previously to be important for the maintenance of cellular homeostasis, specifically under situations of altered cellular pH (Hurth et al., 2005), we decided to explore the metabolic changes in *tdt* plants by conducting a detailed metabolic analysis in leaves and in guard cell-enriched epidermal fragments of the mutant and wild-type plants. There were no significant changes in the levels of chlorophylls (Supplemental Fig. S7). Similarly, during the light/dark cycle, changes were not observed in the leaf levels of Glc, Fru, and Suc between mutant and wild-type plants (Supplemental Fig. S8). However, starch metabolism in the leaves was strongly affected in *tdt* plants during the diurnal cycle (Fig. 3A). Notably, the average starch synthesis and degradation rates were estimated as the difference between starch at the end of the day and the end of the night, divided by the length of the light period or the night, respectively. Starch synthesis rates were 53% (1.43 μmol Glc g^{-1} fresh weight h^{-1}) and 46% (1.64 μmol Glc g^{-1} fresh weight h^{-1}) lower in *tdt-1* and *tdt-2* plants by comparison

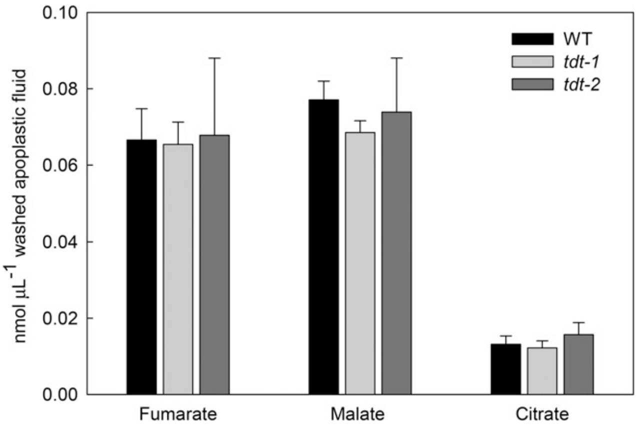

Figure 2. Apoplastic concentrations of organic acids in *tdt* plants. The apoplastic concentrations of fumarate, malate, and citrate were determined as described in "Materials and Methods." Values are presented as means ± SE of six individual determinations per genotype. All measurements were performed in 5-week-old plants. WT, Wild type.

with the wild type (3.04 μmol Glc g^{-1} fresh weight h^{-1}), respectively. For starch degradation rates, the values were on average 59% (0.64 μmol Glc g^{-1} fresh weight h^{-1}) and 48% (0.82 μmol Glc g^{-1} fresh weight h^{-1}) lower in *tdt-1* and *tdt-2* plants than in wild-type plants (1.58 μmol Glc g^{-1} fresh weight h^{-1}), respectively. It should be remembered that the lower levels of starch observed in *tdt* plants were not accompanied by any change A_N.

Impaired accumulation of malate and fumarate was observed previously in *tdt* mutant leaves (Emmerlich et al., 2003; Hurth et al., 2005). We additionally evaluated the malate and fumarate accumulation/usage pattern (Fig. 3). Furthermore, by combining nonaqueous fractionation (NAF) and quantification by enzymatic assays and GC-MS, we were able to estimate their subcellular distribution as well as that of other organic acids (Supplemental Table S5). Regarding the malate and fumarate accumulation during the diurnal cycle, it showed a very similar pattern to that observed for starch, with values observed in *tdt* plants being consistently lower than in the wild type during the entire diurnal cycle. Remarkably, *tdt* plants showed decreases in both malate (Fig. 3B) and fumarate (Fig. 3C), on average of 62% and 44% at the end of the light period. Interestingly, malate was the only organic acid showing differences in its subcellular distribution. Whereas citrate, isocitrate, and fumarate were found predominantly in the vacuoles, malate was reduced significantly in the vacuoles, although increases in malate were observed in the cytosol of the mutant lines (Supplemental Table S5).

We next decided to perform a detailed analysis of the primary metabolism in leaves and in guard cell-enriched epidermal fragments by using the established GC-MS approach (Lisec et al., 2006). This analysis revealed that, among the 48 successfully annotated compounds, considerable changes in amino acids, as well as in both tricarboxylic acid cycle and photorespiratory intermediaries, were observed (Fig. 4; Supplemental Table S6). By analyzing individual amino acids, we observed significant increases in leaves for both lines in Asn, Asp, and Lys levels as well as in the branched chain amino acids Leu and Ile, and the aromatic amino acid Tyr also was increased in the *tdt* plants. Notably, glycolate and Gly, intermediates of the photorespiratory pathway, were decreased significantly in leaves, whereas Gln levels increased in mutant plants in both leaves and guard cells. The levels of some organic acids found in the first half of the tricarboxylic acid cycle citrate (only in leaves) and isocitrate (in both leaves and guard cells) were increased strongly, while succinate, fumarate, and malate were reduced in mutant lines only in leaves. Other changes of note observed in the metabolite profile were the significant increases in myoinositol and reductions in maltose levels in leaves of both lines. Intriguingly, significant increases were observed in the levels of Glc, Fru, and trehalose in guard cells.

We next evaluated whether the metabolic perturbations observed were accompanied by changes in the activity of important enzymes in leaves, which are associated with glycolysis and carbohydrate metabolism (Table III). Interestingly, the maximum activities of PGK, pyruvate kinase, and aldolase (significantly only for *tdt-2*) were higher in *tdt* than in wild-type plants. There were no changes in the activities of hexokinase, phosphofructokinase, enolase, or TPI. Similarly, trans-aldolase and G6PDH, both related to the pentose phosphate pathway, and Suc synthase were unaltered in *tdt* plants. However, the activity of acid invertase was decreased in the mutant lines.

Table II. *Gas-exchange and chlorophyll* a *fluorescence parameters in wild-type and tdt mutant plants measured under growth irradiance (150 μmol m^{-2} s^{-1})*

Data presented are means ± SE (n = 10) obtained in two independent assays (five plants in each assay). A_N, Net photosynthesis; E, transpiration, F_V/F_m, PSII maximum photochemical efficiency.

Parameters	Wild Type	*tdt-1*	*tdt-2*
A_N (μmol CO_2 m^{-2} s^{-1})	5.4 ± 0.2	5.9 ± 0.1	5.6 ± 0.2
g_s (mol water m^{-2} s^{-1})	0.19 ± 0.01	0.18 ± 0.01	0.20 ± 0.01
E (mmol water m^{-2} s^{-1})	1.9 ± 0.2	1.7 ± 0.1	1.9 ± 0.2
F_V/F_m	0.78 ± 0.02	0.76 ± 0.01	0.75 ± 0.01

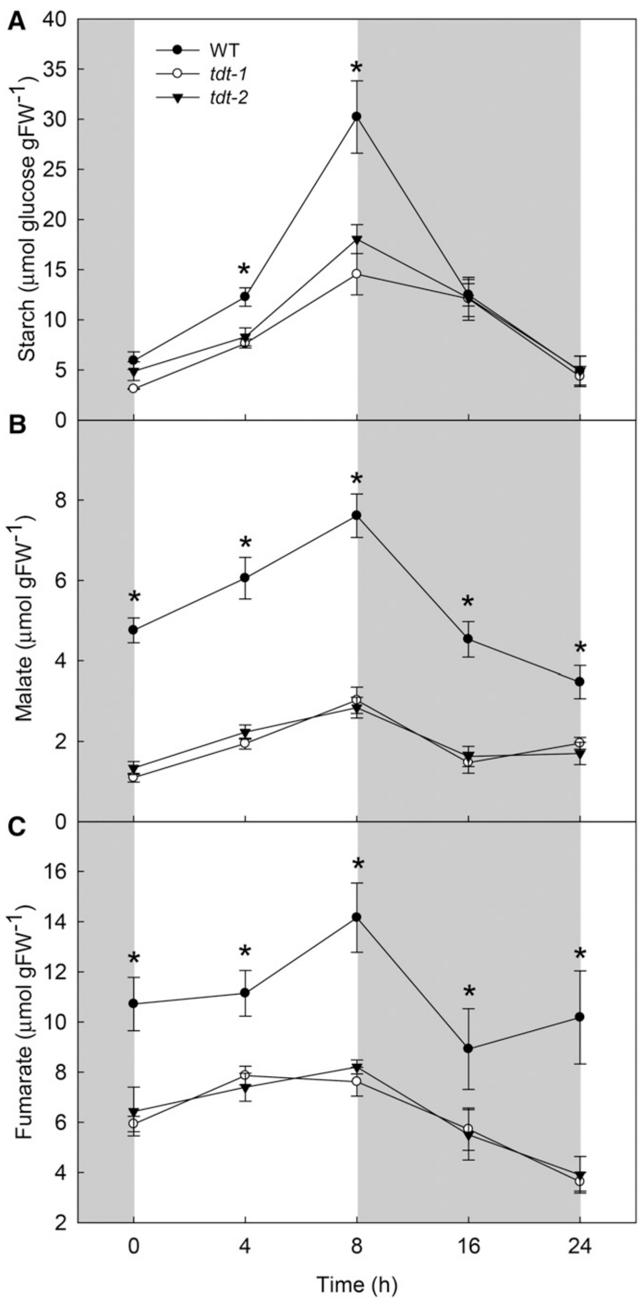

Figure 3. Starch and organic acid contents in wild-type (WT) and *tdt* plants. Starch (A), malate (B), and fumarate (C) contents were determined in whole rosettes harvested at different time points during the light/dark cycle. Values are presented as means ± SE (n = 6), and asterisks indicate times where the values from mutant lines were determined by Student's t test to be significantly different ($P < 0.05$) from the wild type. FW, Fresh weight.

tdt Knockout Plants Present Altered Flux through the Tricarboxylic Acid Cycle

We decided to directly assess the respiration rate by performing two complementary approaches. First, we directly evaluated the rate of light respiration in the mutant lines by measuring the $^{14}CO_2$ evolution following incubation of leaf discs with positionally labeled [^{14}C]Glc molecules to assess the relative rate of flux through the tricarboxylic acid cycle. For this, we incubated leaf discs under light supplied with either [1-^{14}C]Glc or [3,4-^{14}C]Glc over a period of 6 h. During that period, we collected the $^{14}CO_2$ evolved at hourly intervals. CO_2 can be released from the C1 position by the action of enzymes that are not associated with mitochondrial respiration, but CO_2 released from the C3,4 positions of Glc cannot (Nunes-Nesi et al., 2007). Therefore, the ratio of CO_2 evolution from C3,4 to C1 positions provides a reliable indication of the relative rate of the tricarboxylic acid cycle versus other carbohydrate oxidation processes. By comparing the $^{14}CO_2$ release from mutant lines and wild-type plants, we observed that significant increases occurred only for the *tdt-2* line after 5 h of incubation with [1-^{14}C]Glc (Fig. 5A), whereas, when supplied with [3,4-^{14}C]Glc, the $^{14}CO_2$ release was increased significantly in both mutant lines from 4 h onward (Fig. 5B). In addition, the C3,4/C1 ratio was higher in mutant lines than in wild-type plants after 6 h of incubation (Fig. 5C), revealing that a higher proportion of carbohydrate oxidation was performed by the tricarboxylic acid cycle in illuminated leaves. Furthermore, the higher dark respiration, measured by using an infrared gas analyzer system, revealed higher rates of CO_2 evolution in the leaves of *tdt* plants than in the wild type (Fig. 5D).

DISCUSSION

Functional Absence of tDT Does Not Alter Stomatal Movements and Photosynthetic Capacity

To evaluate the reasons underlying the growth impairment observed in *tdt* plants under short-day conditions (Table I; Supplemental Fig. S1), we decided to investigate whether the impaired organic acid accumulation affected stomatal function and, thereby, photosynthetic capacity in these plants. We were somewhat surprised to find that the growth phenotype was independent of changes in stomatal density, stomatal index, and photosynthetic capacity (Tables I and II; Supplemental Fig. S6; Supplemental Tables S2–S4). Collectively, these results indicate that guard cell function is not highly affected in *tdt* plants (Fig. 1), and the stomata were most likely able to reprogram their metabolism to overcome the impaired vacuolar malate storage observed previously (Emmerlich et al., 2003), confirmed here during the entire diurnal cycle and in the nonaqueous fractionation experiments (Fig. 3; Supplemental Table S5). Notably, although tDT is essential for mediating correct compartmentation of the dicarboxylates, *tdt* plants still exhibit residual malate-importing activity (Emmerlich et al., 2003; Hurth et al., 2005). It has been suggested that tDT is the major transporter responsible for malate and fumarate through the tonoplast in mesophyll cells (Hurth et al., 2005);

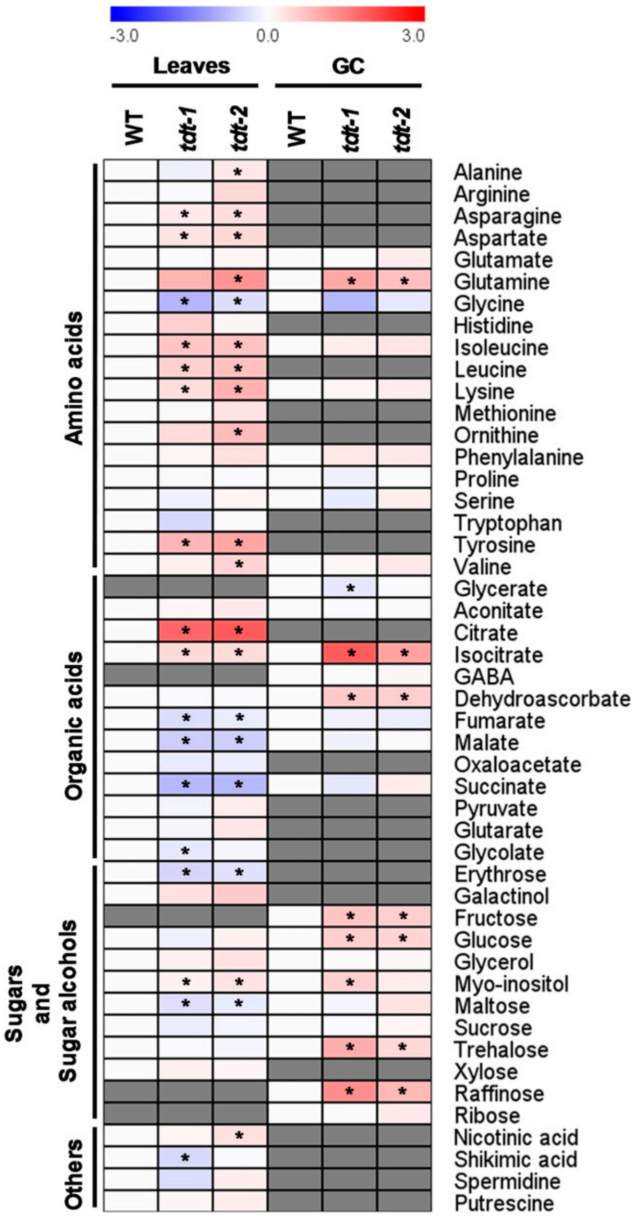

Figure 4. Heat map representing the changes in relative metabolite contents in leaves and guard cell-enriched epidermal fragments (GC) from wild-type (WT) and *tdt* plants. The full data sets from these metabolic profiling studies are available in Supplemental Table S6. The color code of the heat map is given at the $\log_2$ following the scale above the diagram. Data are normalized with respect to the mean response calculated for the wild type (to allow statistical assessment, individual plants from this set were normalized in the same way). Values are presented as means ± SE ($n = 5$). Asterisks indicate that the values from mutant lines were determined by Student's t test to be significantly different ($P < 0.05$) from the wild type. Gray cells indicate metabolites that were not detected or could not be annotated. GABA, γ-Aminobutyrate.

however, members of the ALMT family also are implicated in this function as malate channels in plants. For instance, ALMT6, which is more expressed in guard cells than in mesophyll cells (Supplemental Fig. S3), was shown to mediate Ca^{2+}- and pH-dependent malate currents into guard cell vacuoles, suggesting that it could be the main vacuolar transport system for organic acids in guard cells (Meyer et al., 2011). Because this channel does not exhibit sufficient activity to accumulate dicarboxylates at concentrations required for normal metabolic functioning, it may not be able to fully compensate for the absence of tDT in mesophyll cells (Hurth et al., 2005). Furthermore, ALMT9 was first observed to mediate malate and fumarate currents directed into the vacuole; it was later shown to mediate malate-induced chloride current, which also is important for stomatal opening (Kovermann et al., 2007; De Angeli et al., 2013). Notably, our gene expression analyses did not reveal any significant difference at the mRNA levels of ALMT6 and ALMT9 between wild-type and *tdt* plants (Supplemental Fig. S5).

We demonstrated previously that there is a negative correlation between the apoplastic levels of malate and fumarate and both stomatal aperture and gas exchange in tomato antisense lines for genes encoding fumarase and succinate dehydrogenase enzymes (Araújo et al., 2011). Consistent with the lack of change in stomatal function, in this study, we did not observe any change in apoplastic levels of fumarate, malate, and citrate (Fig. 2). In keeping with this, it is highly tempting to suggest that, although malate and fumarate cannot be accumulated properly in the vacuoles due to the lack of a functional tDT transporter, the majority of these compounds produced need to be redistributed further within the cell. This would support the proper stomatal function by the maintenance of apoplastic concentrations of organic acids even with decreased total amounts in the leaves (Fig. 3). Moreover, it also indicates that these compounds are highly metabolized by the tricarboxylic acid cycle (Fig. 5), as suggested previously (Emmerlich et al., 2003). Thus, it seems that mitochondrial metabolism, especially of those pathways associated with malate, has great potential to improve photosynthesis, and growth ultimately, most likely through a better control of stomatal movements (Nunes-Nesi et al., 2011). That said, it remains to be elucidated whether the functional redundancy in the vacuolar organic acid transport in guard cells is responsible for the lack of stomatal phenotype in *tdt* plants.

Lower Growth in *tdt* Plants Was Not Related to Impairments in the Photosynthetic Capacity

A detailed photosynthetic characterization revealed that the lower vegetative growth in *tdt* plants was not due to an impaired photosynthetic capacity. This analysis was necessary despite the lack of change in stomatal behavior, since the rate of CO_2 diffusion through the stomata is not the only constraint to the photosynthetic performance in plants, and the pathway to CO_2 diffusion from stomata to the Rubisco carboxylation sites in the chloroplasts can become an important limiting factor to the photosynthetic process as well

Table III. *Enzyme activity analyses in wild-type and tdt plants*

Activities were determined in whole 5-week-old rosettes harvested at the middle of the light period. Data are presented as means ± SE (n = 5); values in boldface for *tdt* plants were determined by Student's t test to be significantly different ($P < 0.05$) from the wild type. G6PDH, Glc-6-P dehydrogenase; PGK, phosphoglycerate kinase; TPI, triose phosphate isomerase.

Enzymes	Wild Type	*tdt-1*	*tdt-2*
Hexokinase[a]	13.3 ± 0.5	13.6 ± 0.7	14.7 ± 1.2
PGK[a]	10.5 ± 1.2	**14.5 ± 0.6**	**18.4 ± 0.5**
Pyruvate kinase[b]	105.6 ± 8.0	**162.2 ± 17.5**	**175.2 ± 9.6**
Phosphofructokinase[a]	1.6 ± 0.1	1.6 ± 0.1	1.8 ± 0.2
Enolase[a]	8.3 ± 0.5	7.6 ± 0.3	8.2 ± 0.2
TPI[a]	157.7 ± 8.1	144.0 ± 3.1	157.5 ± 4.4
Aldolase[b]	541.8 ± 39.1	676.4 ± 50.1	**837.2 ± 62.1**
Transaldolase[a]	2.0 ± 0.2	2.2 ± 0.1	1.6 ± 0.1
G6PDH[b]	221.9 ± 16.2	239.8 ± 10.2	269.7 ± 14.3
Suc synthase[b]	245.8 ± 16.8	234.0 ± 5.2	245.5 ± 19.0
Acid invertase[a]	46.0 ± 1.4	**32.2 ± 2.4**	**34.9 ± 1.5**

[a]Values expressed in μmol min^{-1} g^{-1} fresh weight. [b]Values expressed in nmol min^{-1} g^{-1} fresh weight.

as the Rubisco carboxylic capacity (Gerhardt et al., 1987; Martins et al., 2013). Our results demonstrated an invariable instantaneous net CO_2 assimilation in *tdt* plants under both growth irradiance and light saturation (Table II; Supplemental Table S2). This also was observed when we estimated the photosynthetic capacity from response curves of A_N to C_i or C_c as well as to PPFD (Supplemental Fig. S6; Supplemental Tables S3 and S4). Arabidopsis plants with highly reduced levels of malate and fumarate due to the overexpression of a maize (*Zea mays*) plastidic NADP-malic enzyme exhibited smaller rosettes with decreased biomass accumulation and thinner leaves when compared with wild-type plants. This was almost certainly the consequence of a reduced photosynthetic performance under short-day conditions in these plants (Zell et al., 2010), suggesting that the long dark period and extremely low levels of malate and fumarate are not sufficient to support the sugar depletion after the usage of carbohydrate stored during the night. Interestingly, these findings were not observed when these plants were grown under long-day conditions (Fahnenstich et al., 2007). Indeed, the rates of starch and organic acid usage during the night correlate with one another and with the relative growth rate, indicating that, although these two carbon sources are regulated independently, their utilization is highly coordinated (Fahnenstich et al., 2007; Gibon et al., 2009; Zell et al., 2010; Sulpice et al., 2014; Figueroa et al., 2016; Lauxmann et al., 2016). Although many of the molecular details concerning the connection between starch and organic acid metabolism in governing plant growth are being revealed (Figueroa et al., 2016), deeper elucidation of how plants and, in particular, crop species adjust their metabolism to support growth will be important and strategic research avenues to be pursued in the near future.

We showed here that *tdt* plants were impaired in their growth under short-day conditions, which can be explained, at least partially, by the reduced malate and fumarate content in the leaves of these plants across the entire diurnal cycle (Fig. 3, B and C). Moreover, starch accumulation in *tdt* mutant lines in our growth conditions was negatively affected, with reduced values at the end of the light period (Fig. 3A). Therefore, it is reasonable to assume that *tdt* plants display a carbon-starvation phenotype when grown under short-day conditions, given that no visible growth phenotype was observed when we grew these mutant plants under a 12-h/12-h light/dark photoperiod (Supplemental Fig. S2).

Respiratory Metabolism Is Changed as a Consequence of the *tDT* Repression

The impaired malate exchange observed in *tdt* plants has been proposed previously to be able to provoke unknown regulatory reactions at the expense of cytosolic energy equivalents (Emmerlich et al., 2003; Hurth et al., 2005). This assumption was further reinforced by the demonstration that radiolabeled malate fed into mutant leaf discs entered the tricarboxylic acid cycle much faster than in wild-type tissues (Emmerlich et al., 2003). Furthermore, the observation that *tdt* leaf discs exhibited both an increased respiratory activity and increased respiratory quotient (Hurth et al., 2005) demonstrated the accelerated usage of cytosolic carboxylic acids as an energy source in plants lacking a functional tDT transporter. Here, we provide compelling evidence that the absence of tDT strongly affects mitochondrial metabolism in vivo. By using complementary approaches, we further confirmed that the slower growth in *tdt* plants was accompanied by enhanced dark and light respiration (Fig. 5), providing more evidence for the connection between tricarboxylic acid cycle functioning and growth (Nunes-Nesi et al., 2007; Araújo et al., 2011). Tomato plants exhibiting

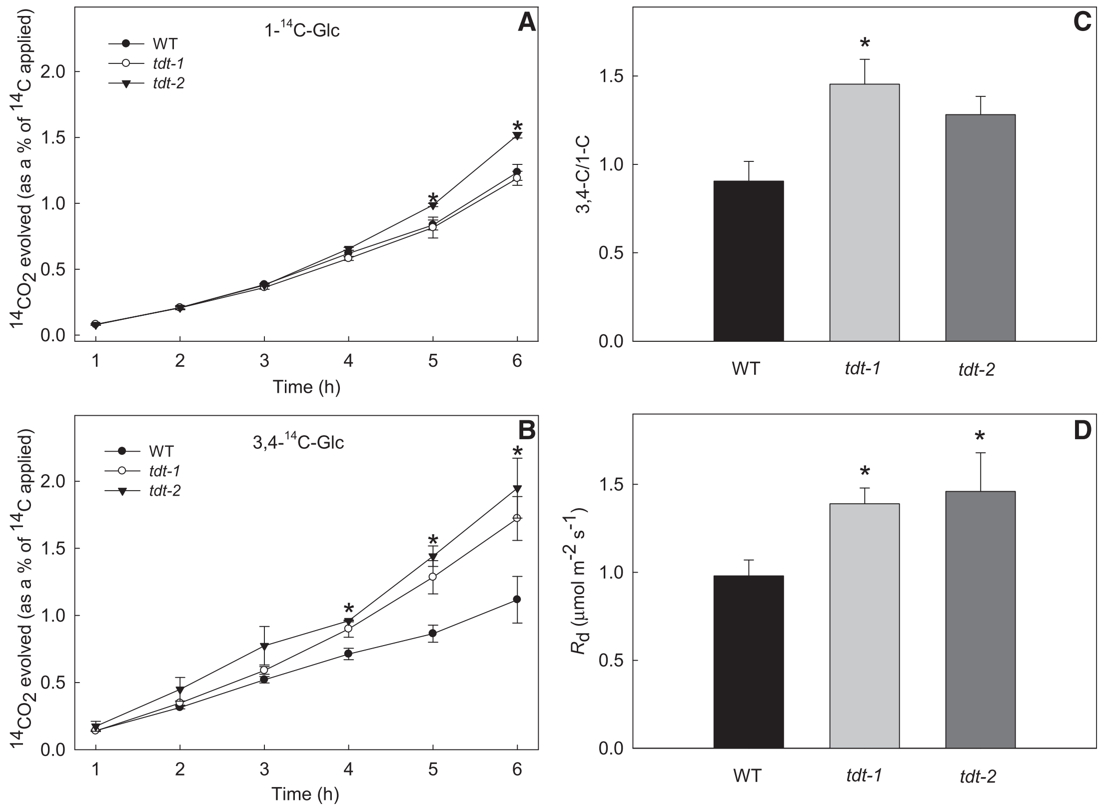

Figure 5. Respiration parameters in leaf discs from wild-type (WT) and *tdt* plants. A and B, $^{14}CO_2$ evolution from isolated leaf discs was determined under light conditions. The leaf discs were taken from 5-week-old plants and incubated in 10 mM MES-KOH solution, pH 6.5, 0.3 mM Glc, and 0.1 mM $CaSO_4$ supplemented with 0.62 kBq mL^{-1} [1-^{14}C]Glc (A) or [3,4-^{14}C]Glc (B) at an irradiance of 100 μmol m^{-2} s^{-1}. The $^{14}CO_2$ released was captured (at hourly intervals) in a KOH trap, and the amount of radiolabel released was quantified subsequently by liquid scintillation counting. C, Ratio of carbon dioxide evolution from C3,4 to C1 positions of Glc in leaves of *tdt* plants. Values are presented as means ± SE (n = 3). D, Dark respiration measurements performed on 5-week-old plants. Values presented are means ± SE (n = 10) obtained in two independent assays (five plants in each assay). Asterisks indicate values that were determined by Student's t test to be significantly different ($P < 0.05$) from the wild type.

either an antisense inhibition of fumarase (Nunes-Nesi et al., 2007) or the iron-sulfur subunit of succinate dehydrogenase (Araújo et al., 2011) displayed impaired mitochondrial metabolism. In these transgenic plants, the flux through the tricarboxylic acid cycle was clearly reduced; however, whereas deficiency in fumarase led to lower CO_2 assimilation and reduction in growth (Nunes-Nesi et al., 2007), the succinate dehydrogenase antisense lines showed higher transpiration and g_s, followed by elevated CO_2 assimilation and growth (Araújo et al., 2011). These differences were both ascribed to the apoplastic levels of malate and fumarate, as mentioned above, which were elevated in the fumarase antisense lines and reduced in the succinate dehydrogenase antisense lines (Araújo et al., 2011). That respiratory metabolism was affected in these lines is by no means surprising, given that they are affected directly in the tricarboxylic acid cycle. That the *tdt* lines also are affected is highly interesting, since it suggests that the tricarboxylic acid cycle is, to a considerable extent, fueled directly by malate supply, which is accumulated in the cytosol in these plants (Supplemental Table S5). Moreover, it is in keeping with previous suggestions of a noncyclic flux mode of the tricarboxylic acid cycle in leaves under light conditions (Sweetlove et al., 2010; António et al., 2016). This scenario is further supported by the steady-state levels of the intermediates of the tricarboxylic acid cycle in leaves observed here (Fig. 4; Supplemental Table S6) and is in good agreement with the high dependence on the metabolic and physiological cell demands associated with organic acid metabolism (Sweetlove et al., 2010).

It is important to highlight that the levels of succinate, fumarate, and malate were decreased in leaves, but not in guard cells, of mutant lines (Fig. 4). This observation suggests a different functional importance of the tDT transporter in mesophyll and guard cells, which is in agreement with the differential expression pattern of *tDT*, being more expressed in mesophyll cells than in guard cells (Bates et al., 2012; Supplemental Fig. S4). Moreover, the high expression of ALMT6 at the guard cell tonoplast seems to compensate for the lack of tDT, at least regarding the proper storage of malate and fumarate in those cells (Fig. 4). Curiously, since we observed a strong accumulation of citrate in leaves and isocitrate in both leaves and guard cells and this accumulation is addressed occurring within the vacuole (Supplemental Table S5), it is tempting to speculate that tDT also might be somehow involved with the compartmentalization of these organic acids. Although we were not able to ascertain in this study which organic acids are effectively transported by the tDT, it will be interesting to investigate in future studies whether the mitochondrial metabolism in guard cells also is affected when tDT is repressed.

Collectively, our results suggest that the impaired accumulation of malate and fumarate as a consequence of nonfunctional tDT affects the cellular homeostasis in mesophyll cells by changing mitochondrial metabolism, without negative impacts to the stomatal and photosynthetic behaviors. When the relative concentrations of the apoplastic and subcellular malate pools are considered (Gerhardt et al., 1987; Winter et al., 1993, 1994; Hedrich et al., 1994; Martinoia and Rentsch, 1994; Lohaus et al., 2001), it is tempting to speculate that the impact on mitochondrial metabolism is most likely due to increased consumption of carboxylates within the cell, since it cannot be properly stored in the vacuole. Additionally, transporting the increased cytosolic malate pools for the maintenance of apoplastic levels could be a mechanism by which *tdt* plants maintain stomatal function. This observation is thus consistent with our previous studies, both suggesting that apoplastic malate levels play a crucial role in stomatal function.

MATERIALS AND METHODS

Plant Material and Growth Conditions

All Arabidopsis (*Arabidopsis thaliana*) plants used here were of the Wassilewskija ecotype background. Wild-type and *tdt* plants were grown in a growth chamber under short-day (8 h/16 h of light/dark) or neutral-day (12 h/12 h of light/dark) irradiance of 150 μmol m^2 s^{-1}, 22°C/20°C during the light/dark cycle, and 60% relative humidity. The T-DNA mutant lines *tdt-1* and *tdt-2* were identified by screening a library of T-DNA lines from the Arabidopsis Knockout Facility, University of Wisconsin Biotechnology Center (Emmerlich et al., 2003). The abundance of transcripts was confirmed by semiquantitative PCR using a specific primer pair for the *tDT* gene (At5g47560): forward, 5′-ACACTACAACATCCATCGCC-3′, and reverse, 5′-ATGCATCCACATGCTTACGT-3′. *GLYCERALDEHYDE-3-PHOSPHATE-DEHYDROGENASE* (At1g16300) expression also was evaluated as a control using the following primer pair: forward, 5′-TGGTTGATCTCGTTGTGCAGGTCTC-3′, and reverse, 5′-GTCAGCCAAGTCAACAACTCTCTG-3′.

Growth Analysis

Whole rosettes from 5-week-old plants were harvested, and the rosette fresh and dry weight, LA, and SLA were measured. LA was measured by a digital image method using a scanner (Hewlett Packard Scanjet G2410), and the images were processed using ImageJ software (Schindelin et al., 2015). SLA was calculated as described by Hunt et al. (2002).

Stomatal Analysis

After 2 h of illumination in the light/dark cycle, leaf impressions were taken from the abaxial surface of the fifth leaf totally expanded with dental resin imprints (Berger and Altmann, 2000). Nail polish copies were made using a colorless glaze (Von Groll et al., 2002), and the images were taken with a digital camera (Axiocam MRc) attached to a microscope (Zeiss; model AX10). The measurements were performed on the images using AxionVision software (Carls Zeiss). Stomatal density and stomatal index (the ratio of stomata to stomata plus other epidermal cells) were determined in at least 10 fields of 0.09 mm^2 per leaf from eight different plants. For the stomatal aperture assay, the totally expanded fifth leaf of 5-week-old plants was floated on stomatal opening buffer containing 10 mM KCl, 50 μM $CaCl_2$, and 5 mM MES-Tris (pH 6.15) for 2 h under light (150 μmol m^{-2} s^{-1}) to preopen stomata. Afterward, ABA, malate, fumarate, citrate, or ethanol (solvent control) was added to the opening buffer to a final concentration of 10 μM, 10 mM, 10 mM, 10 mM, or 0.1% (v/v), respectively. After 2 h of incubation, the stomatal aperture was evaluated. The leaves were gently dried, and the adaxial epidermis was carefully fixed to an autoclave tape. The abaxial surface of the leaves was then peeled off by fixing an adhesive film (tesafilm crystal clear; Tesa), and the images were taken immediately (Azoulay-Shemer et al., 2015). Six leaves from different plants were evaluated, and the aperture of at least 20 stomata per leaf was measured, giving a total of at least 120 stomata per genotype.

Stomatal Opening and Closing Kinetics Measurements

The g_s values were recorded at intervals of 1 min using an open-flow infrared gas-exchange analyzer system (LI-6400XT; LI-COR) equipped with an integrated fluorescence chamber (LI-6400-40; LI-COR). The g_s responses to dark/light and light/dark transitions were measured in plants acclimated to dark or light for at least 2 h. The light in the chamber was kept turned off/then turned on for 10/40 min and turned on/turned off 10/40 min. The CO_2 concentration in the chamber was kept at 400 μmol mol^{-1} air. For responses to CO_2 concentration transitions, leaves were exposed to 400/800/400 μmol CO_2 mol^{-1} air for 10/40/40 min under PPFD of 150 μmol m^{-2} s^{-1} (Medeiros et al., 2016). The half-times, expressed in min, for the stomatal kinetics curves were calculated as $\ln(2)/k$. The rate constant, k, was fitted by nonlinear fitting using Microsoft Excel's Solver add-in as described previously (Martins et al., 2016).

Guard Cell-Enriched Epidermal Fragments and Mesophyll Cell Protoplast Isolation

The isolation of guard cell-enriched epidermal fragments was performed as described previously (Pandey et al., 2002). Briefly, fully expanded leaves from five rosettes per sample were blended for 1 min plus 1 min (twice for 30 s) using a Waring blender (Phillips; RI 2044) with an internal filter to clarify the epidermal fragments of mesophyll and fibrous cells. Subsequently, epidermal fragments were collected on a nylon membrane (200-μm mesh) and washed to avoid apoplast contamination before being frozen in liquid nitrogen. This protocol resulted in a guard cell purity of approximately 98% (Antunes et al., 2012). For mesophyll cell protoplast isolation, approximately 20 fully expanded leaves per replicate were harvested at the middle of the light period. The protoplasts were isolated using the TAPE-sandwich method as described by Wu et al. (2009).

qRT-PCR

qRT-PCR analysis was performed with total RNA isolated from mature leaves using the TRizol reagent (Ambion, Life Technology) following the manufacturer's manual. For guard cell-enriched fragments and mesophyll cell protoplast, the total RNA was isolated using the NucleoSpin RNA Plant Kit (Macherey-Nagel). The integrity of the RNA was checked on 1% (w/v) agarose gels, and the concentration was measured using the QIAxpert system (Qiagen). Digestion with DNase I (Amplication Grade DNase I; Invitrogen) was performed according to the manufacturer's instructions. Subsequently, total RNA was reverse transcribed into cDNA using the Universal RiboClone cDNA Synthesis System (Promega) according to the respective manufacturer's protocols. For the analysis of gene expression, the Fast SYBR Green PCR Master Mix was used with the MicroAmp Optical 96-Well Reaction Plate and MicroAmp Optical Adhesive Film (Applied Biosystems). The relative expression levels were normalized using the constitutively expressed genes *F-BOX* and *TIP41-LIKE* (Czechowski et al., 2005) and calculated using the ΔCt method. The primers used for qRT-PCR were designed using QuantPrime software (Messinger et al., 2006) or taken from those described by De Angeli et al. (2013). Detailed primer information is described in Supplemental Table S1. The following genes were analyzed: *ALMT6* and *ALMT9*; *QUICK ANION CHANNEL1* (*QUAC1*; Medeiros et al., 2016); *ARABIDOPSIS THALIANA ATP-BINDING CASSETTE B14* (*AtABCB14*; Lee et al., 2008); *SLAC1*; *AHA1*, *AHA2*, and *AHA5* (Ueno et al., 2005); *POTASSIUM CHANNEL IN ARABIDOPSIS THALIANA1* (*KAT1*; Nakamura et al., 1995) and *KAT2* (Pilot et al., 2001); *K⁺ TRANSPORTER1* (*AKT1*; Cao et al., 1995); the K^+ outflow channel *GATED OUTWARDLY RECTIFYING K⁺ CHANNEL* (GORK; Ache et al., 2000); and *TWO-PORE CHANNEL1* (*TPC1*; Peiter et al., 2005).

Collection of Apoplastic Fluid and Organic Acid Quantification

The leaf apoplastic fluid was collected as described previously with few modifications (Madsen et al., 2016). Briefly, six completely expanded leaves were cut with a razor blade and submerged immediately in deionized water to remove any surface contaminants at the middle of the light period. Afterward, the leaves were submerged in the washing solution (deionized water). Then, a vacuum was applied to infiltrate the leaves (approximately −70 kPa) and released slowly (this procedure was repeated three times [1 min each] to give 100% infiltration). After vacuum infiltration, leaf surfaces were completely and gently dried. Leaves were placed on a Parafilm sheet, which was folded in such way that the leaves were stacked between layers of Parafilm. Finally, this leaf-Parafilm sandwich was mounted as described (Madsen et al., 2016), and after centrifugation in swinging buckets at 300*g* for 10 min at 4°C, the volume of apoplastic washing fluid was measured with a pipette. The apoplastic washing solutions were dried in a lyophilizer. By using standards for citrate, malate, and fumarate, we were able to quantify the absolute amount of these organic acids in the apoplastic fraction using an established GC-MS approach (Lisec et al., 2006). Epidermis extraction was done by using intact epidermis imaging (instead of blending), whereas the abaxial side of leaves was gently pressed onto a coverslip with a very thin coating of medical adhesive (Hollister). Upper cell layers were carefully removed using a razor blade.

Gas-Exchange and Chlorophyll Fluorescence Measurements

Gas-exchange parameters were determined simultaneously with chlorophyll *a* (Chl *a*) fluorescence measurements using the same gas-exchange system described above. Instantaneous gas exchanges were measured after 1 h of illumination during the light period under 150 μmol m^{-2} s^{-1} (light of growth) or 1,000 μmol m^{-2} s^{-1} (light saturation) PPFD at the leaf level. The reference CO_2 concentration was set at 400 μmol CO_2 mol^{-1} air. All measurements were performed using the 2-cm^2 leaf chamber at 25°C, while the amount of blue light was set to 10% PPFD to optimize stomatal aperture.

All the Chl *a* fluorescence parameters were measured exactly as described by Medeiros et al. (2016). As the actual PSII photochemical efficiency (ϕ_{PSII}), estimated by Chl *a* fluorescence parameters, represents the number of electrons transferred per photon absorbed in the PSII, the electron transport rate (J_{flu}) was calculated as $J_{flu} = \phi_{PSII} \times \alpha \times \beta \times PPFD$, where ? is leaf absorptance and ? reflects the partitioning of absorbed quanta between PSII and PSI, and the product ?? was adopted as in the Arabidopsis literature as 0.451 (Flexas et al., 2007).

Dark respiration (R_d) was measured using the same gas-exchange system as described above after at least 1 h during the dark period, and it was divided by 2 ($R_d/2$) to estimate the mitochondrial respiration rate in the light (Niinemets et al., 2005, 2006, 2009).

Photosynthetic light-response curves (A/PPFD) were initiated at C_a of 400 μmol mol^{-1} and PPFD of 1,000 μmol m^{-2} s^{-1}. Then, the PPFD was increased to 1,200 μmol m^{-2} s^{-1} and afterward decreased stepwise to 0 μmol m^{-2} s^{-1} (13 different PPFD steps). Simultaneously, Chl *a* fluorescence parameters were obtained (Yin et al., 2009). The responses of A_N to C_i (A_N/C_i curves) were determined at saturated light of 1,000 μmol m^{-2} s^{-1} at 25°C under ambient oxygen. Briefly, the measurements started at C_a of 400 μmol mol^{-1}, and when the steady state was reached, C_a was decreased stepwise to 50 μmol mol^{-1}. Upon completion of the measurements at low C_a, C_a was returned to 400 μmol mol^{-1} to restore the original A_N. Next, C_a was increased stepwise to 1,600 μmol mol^{-1} in a total of 13 different C_a values (Long and Bernacchi, 2003).

Estimation of g_m, V_{cmax}, J_{max}, and Photosynthetic Limitations

The C_c was calculated following Harley et al. (1992) as:

$$C_c = (\Gamma^* \ (J_{flu} + 8(A_N + R_L)))/(J_{flu} - 4(A_N + R_L))$$

where the conservative value of Γ^* for Arabidopsis was taken from Mott et al. (2008). Then, g_m was estimated as the slope of the A_N versus $C_i - C_c$ relationship as:

$$g_m = A_N/(C_i - C_c)$$

Thus, estimated g_m is an averaged value over the points used in the relationship ($C_i < 300$ μmol mol^{-1}).

g_m also was estimated by a second method (Ethier and Livingston, 2004), which fits A_N/C_i curves with a nonrectangular hyperbola version Farquhar-von Caemmerer-Berry model, based on the hypothesis that g_m reduces the curvature of the Rubisco-limited portion of an A_N/C_i curve.

From A_N/C_i and A_N/C_c curves, the V_{cmax} and the J_{max} were calculated by fitting the mechanistic model of CO_2 assimilation (Farquhar et al., 1980) using the C_i- or C_c-based temperature dependence of kinetic parameters of Rubisco (K_c and K_o; Mott et al., 2008). Then, V_{cmax}, J_{max}, and g_m were normalized to 25°C using the temperature-response equations from Sharkey et al. (2007).

Determination of Metabolite Levels

Whole rosettes were harvested at different times during the light/dark cycle (0, 4, 8, 16, and 24 h). Rosettes were flash frozen in liquid nitrogen and stored at −80°C until further analyses. The levels of starch, Suc, Fru, and Glc in the leaf tissues were determined as described previously (Fernie et al., 2001). Malate and fumarate were determined as detailed by Nunes-Nesi et al. (2007). The photosynthetic pigments were determined as described (Porra et al., 1989). The metabolite profiling was carried out in samples harvested at the middle of the day for both leaves (Lisec et al., 2006) and guard cell-enriched epidermal fragments as described previously (Daloso et al., 2015), with some modifications. Specifically, after isolation, the guard cell-enriched epidermal fragments were snap frozen in liquid nitrogen and lyophilized for 1 week. Approximately 30 mg of lyophilized guard cell-enriched epidermal fragments was disrupted by shaking together with metal balls. The extraction was performed using 1 mL of methanol and shaking (1,000 rpm) at 70°C for 15 min, and 60 μL of ribitol (0.2 mg mL^{-1}) was added as an internal standard. The followed extraction and derivatization procedure was performed exactly as described (Daloso et al., 2015). Peaks were annotated manually, and ion intensity was determined by the aid of TagFinder software (Luedemann et al., 2012), using a reference library from the Golm Metabolome Database (Kopka et al., 2005) and following the recommended reporting format (Fernie et al., 2011).

NAF

Five-week-old rosettes grown under short days were harvested (pool of five per replicate) in the middle of the light period, flash frozen, ground to a fine powder at −70°C using a cryogenic grinding robot (Stitt et al., 2007), and stored at −80°C until further use. Approximately 4 g of powder was freeze dried (−80°C) for 1 week. NAF was performed as described (Arrivault et al., 2014; Krueger et al., 2014), and the gradient was divided into eight fractions. After the last centrifugation at 3,200*g* (4°C) for 10 min, the supernatant was discarded to remove the solvent from the fractions. The pellet was resuspended in 7 mL of heptane and divided into six aliquots of equal volume. Finally, the suspension was dried in a vacuum concentrator avoiding heating; aliquots were stored at −80°C until further use. Prior to analysis, the dried pellets were homogenized with the appropriate extraction buffer by the addition of one steel ball bearing and shaking at 25 Hz for 1 min in a ball mill (Retsch MM300; Retsch). Enzyme and metabolite markers (ADP Glc pyrophosphorylase and Rubisco activities for the chloroplast, phospho*enol*pyruvate carboxylase and uridine diphosphate Glc pyrophosphorylase activities for the cytosol, and acid invertase activity and nitrate amounts for the vacuole) were determined as described by Arrivault et al. (2014). Malate and fumarate were quantified via coupled enzymatic assays (Cross et al., 2006). Citrate was quantified via an enzymatic assay adapted from Tompkins and Toffaletti (1982) in samples obtained with chloroform/methanol/water extraction (Arrivault et al., 2009). Aliquots of extracts (10 μL) or standards (10 μL of 0, 125, 250, and 500 μM and

1 mM) were dispensed directly onto a microplate, followed by 100 μL of 50 mM buffer (Tricine/KOH, pH 8) containing 0.1 mM $ZnSO_4$, 0.5 mM NADH, 1.5 units of malate dehydrogenase, and 2.3 units of lactate dehydrogenase. Absorbance was monitored at 340 nm until OD stabilized, 0.014 units of citrate lyase was added, and absorbance was monitored until stable. The other metabolites were measured using the GC-MS method also detailed above. Determination of subcellular distribution was performed using BestFit software (Klie et al., 2011).

Enzyme Activity Measurements

The enzymatic extract was prepared as described previously (Gibon et al., 2004). Then, the maximum activities of PGK, pyruvate kinase, phosphofructokinase, aldolase, G6PDH, and acid invertase were determined as described by Gibon et al. (2004); hexokinase, enolase, and TPI following Fernie et al. (2001); SuSy as described by Zrenner et al. (1995); and trans-aldolase according to Debnam and Emes (1999).

Tricarboxylic Acid Cycle Flux on the Basis of $^{14}CO_2$ Evolution

Estimations of the tricarboxylic acid cycle flux on the basis of $^{14}CO_2$ evolution were performed following the incubation of isolated leaf discs in 10 mM MES-KOH, pH 6.5, containing 0.3 mM Glc and supplied with 0.62 kBq mL^{-1} [1-^{14}C]Glc and [3,4-^{14}C]Glc under 150 μmol photons m^{-2} s^{-1}. The evolved $^{14}CO_2$ was trapped in 10% (w/v) KOH and quantified by a liquid scintillation counter (Beckman LS 6500; Beckman Instruments). The results were interpreted following Rees and Beevers (1960).

Experimental Design and Statistical Analysis

The data were obtained from the experiments using a completely randomized design using three genotypes, with the exception of the stomatal opening and closing kinetics, which were performed in a randomized block design. All data are expressed as means ± SE. Data were tested for significant ($P < 0.05$) differences using Student's *t* tests. All the statistical analyses were performed using the algorithm embedded into Microsoft Excel.

Accession Numbers

The Arabidopsis Genome Initiative locus numbers for the major gene discussed in this article is as follows: tDT (At5g47560).

Supplemental Data

The following supplemental materials are available.

Supplemental Figure S1. Gene expression by semiquantitative RT-PCR.

Supplemental Figure S2. Growth phenotypes of wild-type and *tdt* plants.

Supplemental Figure S3. Transcriptome data in leaves and guard cells dissected manually from Arabidopsis leaves.

Supplemental Figure S4. Relative transcript levels of *tDT*.

Supplemental Figure S5. Relative transcript levels of genes involved in organic and inorganic ion transport in guard cells.

Supplemental Figure S6. A_N curves in response to C_i or C_c in wild-type and *tdt* plants.

Supplemental Figure S7. Total chlorophyll content ($a + b$) as well as the a/b ratio in wild-type and *tdt* plants.

Supplemental Figure S8. Sugar content in wild-type and *tdt* plants.

Supplemental Table S1. Primers utilized for the qRT-PCR.

Supplemental Table S2. Gas-exchange and chlorophyll *a* fluorescence parameters in wild-type and *tdt* plants.

Supplemental Table S3. Photosynthetic parameters from light-response curves in wild-type and *tdt* plants.

Supplemental Table S4. Photosynthetic characterization of *tdt* mutant plants.

Supplemental Table S5. Organic acid subcellular distribution.

Supplemental Table S6. Relative metabolite contents for wild-type and *tdt* plants in leaves and guard cell-enriched epidermal fragments.

ACKNOWLEDGMENTS

We thank Dr. Laíse Rosado, Ina Krahnert, and Manuela Guenther (all from the Max Planck Institute of Molecular Plant Physiology [MPIMP]) for helpful technical support; Acácio Salvador (Universidade Federal de Viçosa) for excellent photographic work; Mark Stitt and Dr. Saleh Alseekh (both from the MPIMP) for discussions regarding the NAF assays and GC-MS analysis, respectively, which were highly valuable in the development of this work; and Samuel V.C. Martins (Universidade Federal de Viçosa) for useful discussions concerning gas-exchange analyses.

Received July 17, 2017; accepted September 10, 2017; published September 12, 2017.

LITERATURE CITED

Ache P, Becker D, Ivashikina N, Dietrich P, Roelfsema MRG, Hedrich R (2000) GORK, a delayed outward rectifier expressed in guard cells of *Arabidopsis thaliana*, is a K^+-selective, K^+-sensing ion channel. FEBS Lett **486:** 93–98

António C, Päpke C, Rocha M, Diab H, Limami AM, Obata T, Fernie AR, van Dongen JT (2016) Regulation of primary metabolism in response to low oxygen availability as revealed by carbon and nitrogen isotope redistribution. Plant Physiol **170:** 43–56

Antunes WC, Provart NJ, Williams TCR, Loureiro ME (2012) Changes in stomatal function and water use efficiency in potato plants with altered sucrolytic activity. Plant Cell Environ **35:** 747–759

Araújo WL, Nunes-Nesi A, Osorio S, Usadel B, Fuentes D, Nagy R, Balbo I, Lehmann M, Studart-Witkowski C, Tohge T, et al (2011) Antisense inhibition of the iron-sulphur subunit of succinate dehydrogenase enhances photosynthesis and growth in tomato via an organic acid-mediated effect on stomatal aperture. Plant Cell **23:** 600–627

Arrivault S, Guenther M, Florian A, Encke B, Feil R, Vosloh D, Lunn JE, Sulpice R, Fernie AR, Stitt M, et al (2014) Dissecting the subcellular compartmentation of proteins and metabolites in Arabidopsis leaves using non-aqueous fractionation. Mol Cell Proteomics **13:** 2246–2259

Arrivault S, Guenther M, Ivakov A, Feil R, Vosloh D, van Dongen JT, Sulpice R, Stitt M (2009) Use of reverse-phase liquid chromatography, linked to tandem mass spectrometry, to profile the Calvin cycle and other metabolic intermediates in Arabidopsis rosettes at different carbon dioxide concentrations. Plant J **59:** 826–839

Azoulay-Shemer T, Palomares A, Bagheri A, Israelsson-Nordstrom M, Engineer CB, Bargmann BOR, Stephan AB, Schroeder JI (2015) Guard cell photosynthesis is critical for stomatal turgor production, yet does not directly mediate CO_2- and ABA-induced stomatal closing. Plant J **83:** 567–581

Bates GW, Rosenthal DM, Sun J, Chattopadhyay M, Peffer E, Yang J, Ort DR, Jones AM (2012) A comparative study of the *Arabidopsis thaliana* guard-cell transcriptome and its modulation by sucrose. PLoS ONE **7:** e49641

Berger D, Altmann T (2000) A subtilisin-like serine protease involved in the regulation of stomatal density and distribution in *Arabidopsis thaliana*. Genes Dev **14:** 1119–1131

Bolwell GP, Bindschedler LV, Blee KA, Butt VS, Davies DR, Gardner SL, Gerrish C, Minibayeva F (2002) The apoplastic oxidative burst in response to biotic stress in plants: a three-component system. J Exp Bot **53:** 1367–1376

Cao Y, Ward JM, Kelly WB, Ichida AM, Gaber RF, Anderson JA, Uozumi N, Schroeder JI, Crawford NM (1995) Multiple genes, tissue specificity, and expression-dependent modulation contribute to the functional diversity of potassium channels in *Arabidopsis thaliana*. Plant Physiol **109:** 1093–1106

Cross JM, von Korff M, Altmann T, Bartzetko L, Sulpice R, Gibon Y, Palacios N, Stitt M (2006) Variation of enzyme activities and metabolite levels in 24 Arabidopsis accessions growing in carbon-limited conditions. Plant Physiol **142:** 1574–1588

Czechowski T, Stitt M, Altmann T, Udvardi MK, Scheible WR (2005) Genome-wide identification and testing of superior reference genes for transcript normalization in Arabidopsis. Plant Physiol **139:** 5–17

Daloso DM, Antunes WC, Pinheiro DP, Waquim JP, Araújo WL, Loureiro ME, Fernie AR, Williams TCR (2015) Tobacco guard cells fix CO_2 by both Rubisco and PEPcase while sucrose acts as a substrate during light-induced stomatal opening. Plant Cell Environ **38:** 2353–2371

De Angeli A, Zhang J, Meyer S, Martinoia E (2013) *At*ALMT9 is a malate-activated vacuolar chloride channel required for stomatal opening in Arabidopsis. Nat Commun **4:** 1804

Debnam PM, Emes MJ (1999) Subcellular distribution of enzymes of the oxidative pentose phosphate pathway in root and leaf tissues. J Exp Bot **50:** 1653–1661

Delhaize E, Gruber BD, Ryan PR (2007) The roles of organic anion permeases in aluminium resistance and mineral nutrition. FEBS Lett **581:** 2255–2262

Emmerlich V, Linka N, Reinhold T, Hurth MA, Traub M, Martinoia E, Neuhaus HE (2003) The plant homolog to the human sodium/dicarboxylic cotransporter is the vacuolar malate carrier. Proc Natl Acad Sci USA **100:** 11122–11126

Ethier GJ, Livingston NJ (2004) On the need to incorporate sensitivity to CO_2 transfer conductance into the Farquhar-von Caemmerer-Berry leaf photosynthesis model. Plant Cell Environ **27:** 137–153

Fahnenstich H, Saigo M, Niessen M, Zanor MI, Andreo CS, Fernie AR, Drincovich MF, Flügge UI, Maurino VG (2007) Alteration of organic acid metabolism in Arabidopsis overexpressing the maize C4 NADP-malic enzyme causes accelerated senescence during extended darkness. Plant Physiol **145:** 640–652

Farquhar GD, von Caemmerer S, Berry JA (1980) A biochemical model of photosynthetic CO_2 assimilation in leaves of C 3 species. Planta **149:** 78–90

Fernie AR, Aharoni A, Willmitzer L, Stitt M, Tohge T, Kopka J, Carroll AJ, Saito K, Fraser PD, DeLuca V (2011) Recommendations for reporting metabolite data. Plant Cell **23:** 2477–2482

Fernie AR, Carrari F, Sweetlove LJ (2004) Respiratory metabolism: glycolysis, the TCA cycle and mitochondrial electron transport. Curr Opin Plant Biol **7:** 254–261

Fernie AR, Roscher A, Ratcliffe RG, Kruger NJ (2001) Fructose 2,6-bisphosphate activates pyrophosphate:fructose-6-phosphate 1-phosphotransferase and increases triose phosphate to hexose phosphate cycling in heterotrophic cells. Planta **212:** 250–263

Figueroa CM, Feil R, Ishihara H, Watanabe M, Kölling K, Krause U, Höhne M, Encke B, Plaxton WC, Zeeman SC, et al (2016) Trehalose 6-phosphate coordinates organic and amino acid metabolism with carbon availability. Plant J **85:** 410–423

Finkemeier I, König AC, Heard W, Nunes-Nesi A, Pham PA, Leister D, Fernie AR, Sweetlove LJ (2013) Transcriptomic analysis of the role of carboxylic acids in metabolite signaling in Arabidopsis leaves. Plant Physiol **162:** 239–253

Flexas J, Ortuño MF, Ribas-Carbo M, Diaz-Espejo A, Flórez-Sarasa ID, Medrano H (2007) Mesophyll conductance to CO_2 in *Arabidopsis thaliana*. New Phytol **175:** 501–511

Gerhardt R, Stitt M, Heldt HW (1987) Subcellular metabolite levels in spinach leaves: regulation of sucrose synthesis during diurnal alterations in photosynthetic partitioning. Plant Physiol **83:** 399–407

Gibon Y, Blaesing OE, Hannemann J, Carillo P, Höhne M, Hendriks JH, Palacios N, Cross J, Selbig J, Stitt M (2004) A Robot-based platform to measure multiple enzyme activities in *Arabidopsis* using a set of cycling assays: comparison of changes of enzyme activities and transcript levels during diurnal cycles and in prolonged darkness. Plant Cell **16:** 3304–3325

Gibon Y, Pyl ET, Sulpice R, Lunn JE, Höhne M, Günther M, Stitt M (2009) Adjustment of growth, starch turnover, protein content and central metabolism to a decrease of the carbon supply when Arabidopsis is grown in very short photoperiods. Plant Cell Environ **32:** 859–874

Harley PC, Loreto F, Di Marco G, Sharkey TD (1992) Theoretical considerations when estimating the mesophyll conductance to CO_2 flux by analysis of the response of photosynthesis to CO_2. Plant Physiol **98:** 1429–1436

Hedrich R, Marten I (1993) Malate-induced feedback regulation of plasma membrane anion channels could provide a CO_2 sensor to guard cells. EMBO J **12:** 897–901

Hedrich R, Marten I, Lohse G, Dietrich P, Winter H, Lohaus G, Heldt HW (1994) Malate-sensitive anion channels enable guard cells to sense changes in the ambient CO_2 concentration. Plant J **6:** 741–748

Hunt R, Causton DR, Shipley B, Askew AP (2002) A modern tool for classical plant growth analysis. Ann Bot (Lond) **90:** 485–488

Hurth MA, Suh SJ, Kretzschmar T, Geis T, Bregante M, Gambale F, Martinoia E, Neuhaus HE (2005) Impaired pH homeostasis in Arabidopsis lacking the vacuolar dicarboxylate transporter and analysis of carboxylic acid transport across the tonoplast. Plant Physiol **137:** 901–910

Kim TH, Böhmer M, Hu H, Nishimura N, Schroeder JI (2010) Guard cell signal transduction network: advances in understanding abscisic acid, CO_2, and Ca^{2+} signaling. Annu Rev Plant Biol **61:** 561–591

Klie S, Krueger S, Krall L, Giavalisco P, Flügge UI, Willmitzer L, Steinhauser D (2011) Analysis of the compartmentalized metabolome: a validation of the non-aqueous fractionation technique. Front Plant Sci **2:** 55

Kopka J, Schauer N, Krueger S, Birkemeyer C, Usadel B, Bergmüller E, Dörmann P, Weckwerth W, Gibon Y, Stitt M, et al (2005) GMD@CSB.DB: the Golm Metabolome Database. Bioinformatics **21:** 1635–1638

Kovermann P, Meyer S, Hörtensteiner S, Picco C, Scholz-Starke J, Ravera S, Lee Y, Martinoia E (2007) The Arabidopsis vacuolar malate channel is a member of the ALMT family. Plant J **52:** 1169–1180

Krueger S, Steinhauser D, Lisec J, Giavalisco P (2014) Analysis of subcellular metabolite distributions within *Arabidopsis thaliana* leaf tissue: a primer for subcellular metabolomics. Methods Mol Biol **1062:** 575–596

Lauxmann MA, Annunziata MG, Brunoud G, Wahl V, Koczut A, Burgos A, Olas JJ, Maximova E, Abel C, Schlereth A, et al (2016) Reproductive failure in *Arabidopsis thaliana* under transient carbohydrate limitation: flowers and very young siliques are jettisoned and the meristem is maintained to allow successful resumption of reproductive growth. Plant Cell Environ **39:** 745–767

Lee M, Choi Y, Burla B, Kim YY, Jeon B, Maeshima M, Yoo JY, Martinoia E, Lee Y (2008) The ABC transporter *At*ABCB14 is a malate importer and modulates stomatal response to CO_2. Nat Cell Biol **10:** 1217–1223

Lisec J, Schauer N, Kopka J, Willmitzer L, Fernie AR (2006) Gas chromatography mass spectrometry-based metabolite profiling in plants. Nat Protoc **1:** 387–396

Lohaus G, Pennewiss K, Sattelmacher B, Hussmann M, Hermann Muehling K (2001) Is the infiltration-centrifugation technique appropriate for the isolation of apoplastic fluid? A critical evaluation with different plant species. Physiol Plant **111:** 457–465

Long SP, Bernacchi CJ (2003) Gas exchange measurements, what can they tell us about the underlying limitations to photosynthesis? Procedures and sources of error. J Exp Bot **54:** 2393–2401

Luedemann A, von Malotky L, Erban A, Kopka J (2012) TagFinder: preprocessing software for the fingerprinting and the profiling of gas chromatography–mass spectrometry based metabolome analyses. *In* NW Hardy, RD Hall, eds, Plant Metabolomics: Methods and Protocols. Humana Press, Totowa, NJ, pp 255–286

Madsen SR, Nour-Eldin HH, Halkier BA (2016) Collection of apoplastic fluids from *Arabidopsis thaliana* leaves. *In* GA Fett-Neto, ed, Biotechnology of Plant Secondary Metabolism: Methods and Protocols. Springer, New York, pp 35–42

Maier A, Zell MB, Maurino VG (2011) Malate decarboxylases: evolution and roles of NAD(P)-ME isoforms in species performing C(4) and C(3) photosynthesis. J Exp Bot **62:** 3061–3069

Martinoia E, Rentsch D (1994) Malate compartmentation: responses to a complex metabolism. Annu Rev Plant Physiol Plant Mol Biol **45:** 447–467

Martins SCV, Galmés J, Molins A, DaMatta FM (2013) Improving the estimation of mesophyll conductance to CO_2: on the role of electron transport rate correction and respiration. J Exp Bot **64:** 3285–3298

Martins SCV, McAdam SA, Deans RM, DaMatta FM, Brodribb TJ (2016) Stomatal dynamics are limited by leaf hydraulics in ferns and conifers: results from simultaneous measurements of liquid and vapour fluxes in leaves. Plant Cell Environ **39:** 694–705

Medeiros DB, Martins SCV, Cavalcanti JHF, Daloso DM, Martinoia E, Nunes-Nesi A, DaMatta FM, Fernie AR, Araújo WL (2016) Enhanced photosynthesis and growth in *atquac1* knockout mutants are due to altered organic acid accumulation and an increase in both stomatal and mesophyll conductance. Plant Physiol **170:** 86–101

Messinger SM, Buckley TN, Mott KA (2006) Evidence for involvement of photosynthetic processes in the stomatal response to CO_2. Plant Physiol **140:** 771–778

Meyer S, Scholz-Starke J, De Angeli A, Kovermann P, Burla B, Gambale F, Martinoia E (2011) Malate transport by the vacuolar *At*ALMT6 channel in guard cells is subject to multiple regulation. Plant J **67:** 247–257

Mott KA, Sibbernsen ED, Shope JC (2008) The role of the mesophyll in stomatal responses to light and CO_2. Plant Cell Environ **31:** 1299–1306

Nakamura RL, McKendree WL Jr, Hirsch RE, Sedbrook JC, Gaber RF, Sussman MR (1995) Expression of an Arabidopsis potassium channel gene in guard cells. Plant Physiol **109:** 371–374

Negi J, Matsuda O, Nagasawa T, Oba Y, Takahashi H, Kawai-Yamada M, Uchimiya H, Hashimoto M, Iba K (2008) CO_2 regulator SLAC1 and its homologues are essential for anion homeostasis in plant cells. Nature **452:** 483–486

Niinemets Ü, Cescatti A, Rodeghiero M, Tosens T (2005) Leaf internal diffusion conductance limits photosynthesis more strongly in older leaves of Mediterranean evergreen broad-leaved species. Plant Cell Environ **28:** 1552–1566

Niinemets U, Cescatti A, Rodeghiero M, Tosens T (2006) Complex adjustments of photosynthetic potentials and internal diffusion conductance to current and previous light availabilities and leaf age in Mediterranean evergreen species *Quercus ilex*. Plant Cell Environ **29:** 1159–1178

Niinemets U, Díaz-Espejo A, Flexas J, Galmés J, Warren CR (2009) Role of mesophyll diffusion conductance in constraining potential photosynthetic productivity in the field. J Exp Bot **60:** 2249–2270

Nunes-Nesi A, Araújo WL, Fernie AR (2011) Targeting mitochondrial metabolism and machinery as a means to enhance photosynthesis. Plant Physiol **155:** 101–107

Nunes-Nesi A, Carrari F, Gibon Y, Sulpice R, Lytovchenko A, Fisahn J, Graham J, Ratcliffe RG, Sweetlove LJ, Fernie AR (2007) Deficiency of mitochondrial fumarase activity in tomato plants impairs photosynthesis via an effect on stomatal function. Plant J **50:** 1093–1106

Pandey S, Wang XQ, Coursol SA, Assmann SM (2002) Preparation and applications of *Arabidopsis thaliana* guard cell protoplasts. New Phytol **153:** 517–526

Peiter E, Maathuis FJM, Mills LN, Knight H, Pelloux J, Hetherington AM, Sanders D (2005) The vacuolar Ca^{2+}-activated channel TPC1 regulates germination and stomatal movement. Nature **434:** 404–408

Pilot G, Lacombe B, Gaymard F, Cherel I, Boucherez J, Thibaud JB, Sentenac H (2001) Guard cell inward K^+ channel activity in Arabidopsis involves expression of the twin channel subunits KAT1 and KAT2. J Biol Chem **276:** 3215–3221

Porra RJ, Thompson WA, Kriedemann PE (1989) Determination of accurate extinction coefficients and simultaneous equations for assaying chlorophylls a and b extracted with four different solvents: verification of the concentration of chlorophyll standards by atomic absorption spectroscopy. Biochim Biophys Acta **975:** 384–394

Raschke K (2003) Alternation of the slow with the quick anion conductance in whole guard cells effected by external malate. Planta **217:** 651–657

Rees TA, Beevers H (1960) Pathways of glucose dissimilation in carrot slices. Plant Physiol **35:** 830–838

Santelia D, Lawson T (2016) Rethinking guard cell metabolism. Plant Physiol **172:** 1371–1392

Schindelin J, Rueden CT, Hiner MC, Eliceiri KW (2015) The ImageJ ecosystem: an open platform for biomedical image analysis. Mol Reprod Dev **82:** 518–529

Sharkey TD, Bernacchi CJ, Farquhar GD, Singsaas EL (2007) Fitting photosynthetic carbon dioxide response curves for C(3) leaves. Plant Cell Environ **30:** 1035–1040

Stitt M, Sulpice R, Gibon Y, Whitwell A, Skilbeck R, Parker S, Ellison R October 7, 2007. Cryogenic grinder system. German Patent Application No. 08146.0025U1

Sulpice R, Flis A, Ivakov AA, Apelt F, Krohn N, Encke B, Abel C, Feil R, Lunn JE, Stitt M (2014) Arabidopsis coordinates the diurnal regulation of carbon allocation and growth across a wide range of photoperiods. Mol Plant **7:** 137–155

Sweetlove LJ, Beard KFM, Nunes-Nesi A, Fernie AR, Ratcliffe RG (2010) Not just a circle: flux modes in the plant TCA cycle. Trends Plant Sci **15:** 462–470

Tompkins D, Toffaletti J (1982) Enzymic determination of citrate in serum and urine, with use of the Worthington "ultrafree" device. Clin Chem **28:** 192–195

Tronconi MA, Fahnenstich H, Gerrard Weehler MC, Andreo CS, Flügge UI, Drincovich MF, Maurino VG (2008) Arabidopsis NAD-malic enzyme functions as a homodimer and heterodimer and has a major impact on nocturnal metabolism. Plant Physiol **146:** 1540–1552

Ueno K, Kinoshita T, Inoue S, Emi T, Shimazaki K (2005) Biochemical characterization of plasma membrane H^+-ATPase activation in guard cell protoplasts of Arabidopsis thaliana in response to blue light. Plant Cell Physiol **46:** 955–963

Von Groll U, Berger D, Altmann T (2002) The subtilisin-like serine protease SDD1 mediates cell-to-cell signaling during *Arabidopsis* stomatal development. Plant Cell **14:** 1527–1539

Weisskopf L, Abou-Mansour E, Fromin N, Tomasi N, Santelia D, Edelkott I, Neumann G, Aragno M, Tabacchi R, Martinoia E (2006) White lupin has developed a complex strategy to limit microbial degradation of secreted citrate required for phosphate acquisition. Plant Cell Environ **29:** 919–927

Winter H, Robinson DG, Heldt HW (1993) Subcellular volumes and metabolite concentrations in barley leaves. Planta **191:** 180–190

Winter H, Robinson DG, Heldt HW (1994) Subcellular volumes and metabolite concentrations in spinach leaves. Planta **193:** 530–535

Wu FH, Shen SC, Lee LY, Lee SH, Chan MT, Lin CS (2009) Tape-Arabidopsis Sandwich: a simpler Arabidopsis protoplast isolation method. Plant Methods **5:** 16

Yin X, Struik PC, Romero P, Harbinson J, Evers JB, van der Putten PEL, Vos J (2009) Using combined measurements of gas exchange and chlorophyll fluorescence to estimate parameters of a biochemical C photosynthesis model: a critical appraisal and a new integrated approach applied to leaves in a wheat (Triticum aestivum) canopy. Plant Cell Environ **32:** 448–464

Zell MB, Fahnenstich H, Maier A, Saigo M, Voznesenskaya EV, Edwards GE, Andreo C, Schleifenbaum F, Zell C, Drincovich MF, et al (2010) Analysis of Arabidopsis with highly reduced levels of malate and fumarate sheds light on the role of these organic acids as storage carbon molecules. Plant Physiol **152:** 1251–1262

Zrenner R, Salanoubat M, Willmitzer L, Sonnewald U (1995) Evidence of the crucial role of sucrose synthase for sink strength using transgenic potato plants (*Solanum tuberosum* L.). Plant J **7:** 97–107